Electron Paramagnetic Resonance and ab Initio Structural Studies on Liquid Crystalline Systems

M. A. Morsy, G. A. Oweimreen,* and A. M. Al-Tawfiq

Department of Chemistry, King Fahd University of Petroleum & Minerals, Dhahran 31261, Saudi Arabia

Received: July 3, 1997; In Final Form: December 3, 1997

Electron paramagnetic resonance studies, using PD-Tempone as a probe, on the *n*-hexyl and *n*-heptyl members of the *p*-cyanophenyl *p*-(*n*-alkyl)benzoate (RCBz) liquid crystals confirm the previously observed directions of the discontinuities in the *a* and *g*-factor values on solidification and on melting of the 6CB liquid crystal. Careful analysis of an unusual variation in the *g*-factor value on cooling and heating in the vicinity of the nematic-to-isotropic transition points to the existence of molecular change alongside the bulk change. Evidence for such changes is provided by the results of differential scanning calorimetry (DSC) measurements and ab initio calculations using the STO-3G basis set. DSC endothermic peaks on cooling (or exothermic peaks on heating) that are independent of cooling (or heating) rates reflect a conformational change. DSC also shows the existence of polymorphic solid that, on heating, undergoes a series of rate-dependent solid−solid modifications until the most stable solid form is reached. The STO-3G ab initio calculations suggest three possible conformers for these liquid crystals.

Introduction

There is marked interest in the properties of liquid crystal systems in light of their extensive practical applications[1,2] and their role in biological systems.[3,4]

Most experimental and theoretical studies are concerned with liquid crystals formed by small organic molecules.[5] It was believed that it is unnecessary to take into account all details of the molecular structure, since even simple models give in many cases a qualitative and even a quantitative description of the most important features of liquid crystals.[6] However, a recent electron paramagnetic resonance (EPR) study,[7] in which the alkylcyanobiphyenyls (RCB's, structure **I**) were probed by predeuterated-2,2,6,6-tetramethyl-4-piperidone-*N*-oxide (PD-Tempone, structure **II**), revealed a behavior in 6CB that was not observed in its 5CB, 7CB, and 8CB homologues. On solidification of the supercooled nematic 6CB at about 11.5 °C,

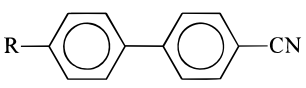

RCB's, Structure I

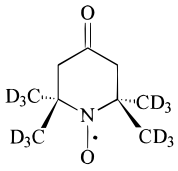

PDT, Structure II

the hyperfine constant, *a*, for the nitroxide PDT probe exhibited a sudden increase to a value comparable to that observed in isotropic 6CB. This *a* value persisted down to about 0 °C. On heating, it remained more or less constant up to about 15.5 °C, which is close to the melting point of 6CB (BDH Chemicals Ltd. report a melting point temperature of 14.5 °C) where it dropped, again suddenly, to a value comparable to that in nematic 6CB. On further heating the variation of *a* with temperature retraced the cooling cycle values. For 5CB, 7CB, and 8CB, the *a* versus *t* values for the heating cycle retraced the *a* versus *t* values for the cooling cycle without undergoing the above-mentioned rise and drop in the *a* values in their supercooled nematic region. This led us to postulate[7] that the nonplanarity of the biphenyl benzene rings is severe enough to disrupt the alignment in supercooled nematic 6CB.

Clearly the transitional properties of liquid crystals are a reflection of their molecular characteristics. To examine the effect of introducing greater flexibility and in turn a greater degree of nonplanarity into the core of the liquid crystal molecule, detailed theoretical and experimental studies were carried out on the *n*-hexyl and *n*-heptyl members of the *p*-cyanophenyl *p*-(*n*-alkyl)benzoate (RCBz, structure **III**) homologous series of liquid crystals which, unlike the RCB's, have cores with an ester group between the two benzene rings.

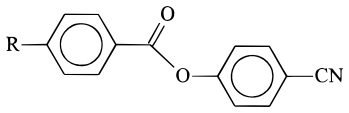

RCBz, Structure III

The results from EPR measurements on 6CBz and 7CBz corroborate recent results for 6CB,[7] which showed that the *g*-factor is strongly dependent on the structure and conformation of the liquid crystal molecule. This finding and the observation in this study of an unusual variation in the *g*-factor value on cooling and heating in the vicinity of the nematic-to-isotropic transition point to an ongoing conformational change during the transition. Differential scanning calorimetric (DSC) thermograms for 6CB, 6CBz, and 7CBz and ab initio calculations on 6CBz and 7CBz support this view and indicate that more than one solid-phase exist for these liquid crystals.

Experimental Section

Materials. The nitroxide spin probe, PD-Tempone (PDT), obtained from Molecular Probes was used without further purification. The liquid crystals 6CBz and 7CBz were obtained

* To whom correspondence should be addressed.

S1089-5647(97)02163-9 CCC: $15.00
Published on Web 04/18/1998

from Hoffmann-La Roche, Inc. They were assessed to be highly pure because they exhibited sharp transition temperatures (to within ±0.1 °C) and were used as supplied.

EPR Spectroscopy. The EPR sample solutions were prepared by introducing the probe (PDT at a mole fraction about 4×10^{-5}) into the melted isotropic liquid crystal. The probed solution was transferred to a preheated EPR Pyrex tube using a very narrow-mouthed disposable dropper until a length just over 1 cm was reached. Such length was needed to minimize the temperature gradient over the entire sample to the order of temperature fluctuations and to ensure that all the sample is within the active region of the microwave cavity.

The choice of the proper spectral parameters for the Brucker ER-200D-SRC series spectrometer and the temperature control apparatus have been described elsewhere.[8]

The EPR experiment was carried out as follows: Initially, the temperature of the sample was raised 10 °C or more above its nematic-to-isotropic transition temperature. Spectra were obtained as the temperature of the isotropic phase was lowered to just below the isotropic-to-nematic transition temperature. After about 10 min, many spectra were obtained at close temperature intervals as the sample was heated to just above the nematic-to-isotropic transition. Spectra were then taken, again at close temperature intervals, as the sample was cooled across the isotropic-to-nematic transition and through the nematic (or supercooled nematic) phase down to a temperature at which the high-field signal of the nitroxide radical probe became comparable to the spectral noise. Finally, a set of spectra were obtained as the sample was heated, at somewhat larger temperature intervals, to cross the melting and nematic-to-isotropic transition temperatures. In all the measurements the sample temperature was kept constant to within ±0.02 °C for at least 10 min. before a spectrum was taken and the temperature decreased or increased for the next spectral measurement.

Differential Scanning Calorimetry (DSC). The thermal properties of 6CB, 6CBz, and 7CBz were studied using a Perkin-Elmer differential scanning calorimeter (DSC-4). High-purity cyclohexane and octadecane (supplied by Fluka) were used to calibrate the temperature and the heat of fusion. All materials studied had a sample weight between 5 and 7 mg. The studies involved repeated heating and cooling thermograms at 10 and 3 °C/min. To investigate the effect of the cooling and heating rates, further 6CB and 6CBz were also run at 1 °C/min. In these runs the temperature ranges were between −30 °C, where all the liquid crystals are in the solid state, and a temperature 10 °C or more above their nematic-to-isotropic transition. Data analysis for all the thermograms was carried out using the TADS data-handling PC-software associated with the DSC-4 unit.

Method of Calculations. With the availability of relatively fast personal computers (PC), it is now possible to carry out rapid ab initio calculations on molecules with 12 or more atoms with different basis sets. However, there are considerable limitations owing to the PC hardware configurations (e.g., RAM and hardware storage capacity).

The HyperChem Model Builder[9] was used to construct an approximate geometry for each of the systems studied. Geometry optimization calculations were initially carried out using the molecular mechanics force field method[10] (MM+), and further refinement in the molecular geometry was achieved using the semiempirical quantum mechanical method[11] (AM1). The *Z*-matrix file created for each of the studied systems from its refined molecular geometry by HyperChem was finally optimized with the GAUSSIAN 94W program[12] with no constraints.

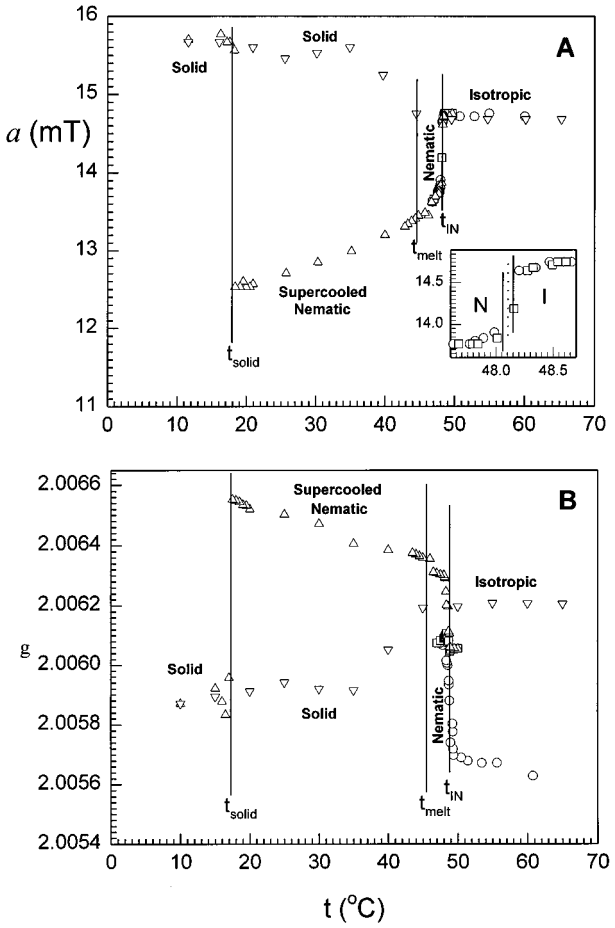

Figure 1. Hyperfine constant *a* (A) and the *g*-factor (B) versus temperature for PDT in 6CBz. The inset in (A) emphasizes the first cooling (○) and heating (□) cycles in the vicinity of the nematic-to-isotropic transition. The variation of *a* and the *g*-factor with temperature is given for the second cooling (△) and heating (▽) runs across the various phases.

The final optimization, to obtain the global minimum for each system, was carried out at the LCAO−MO−SCF restricted Hartree−Fock level with the minimal Pople valence-shell STO-3G[13] basis set. The potential energy surface (PES)[14] was scanned for the 6CBz (and 7CBz) molecule by increasing, in 36 10° steps, the dihedral angle between its cyanophenyl and alkylbenzoate portions (starting from the −50° angle obtained for the molecular global minimum by the STO-3G basis set) and fixing all other structural parameters.

Results and Discussion

EPR Results. Figures 1 and 2 show the variation of the hyperfine constant (*a*) and the *g*-factor values with temperature for PDT in all the phases of 6CBz and 7CBz, respectively. For the sake of clarity and to facilitate the discussion of the results parts A and B of Figure 2 are detailed in parts A−D and A′−D′, respectively, of Figure 3. This figure also reflects the manner in which the EPR experiment was performed.

In an earlier study[7] it was found that the value of the hyperfine constant in the isotropic phase (a_I) is 14.73 mT for the PDT/RCB systems and 15.73 mT for the TP/RCB systems. The difference between the a_I values for PDT and TP was shown to be due to differences in their structures and in turn their interactions with the RCB solvent molecules. PDT is globular, whereas TP has a hexadecanoyloxy tail. The TP radical probes with their long tails tend to correlate with the tails of the liquid

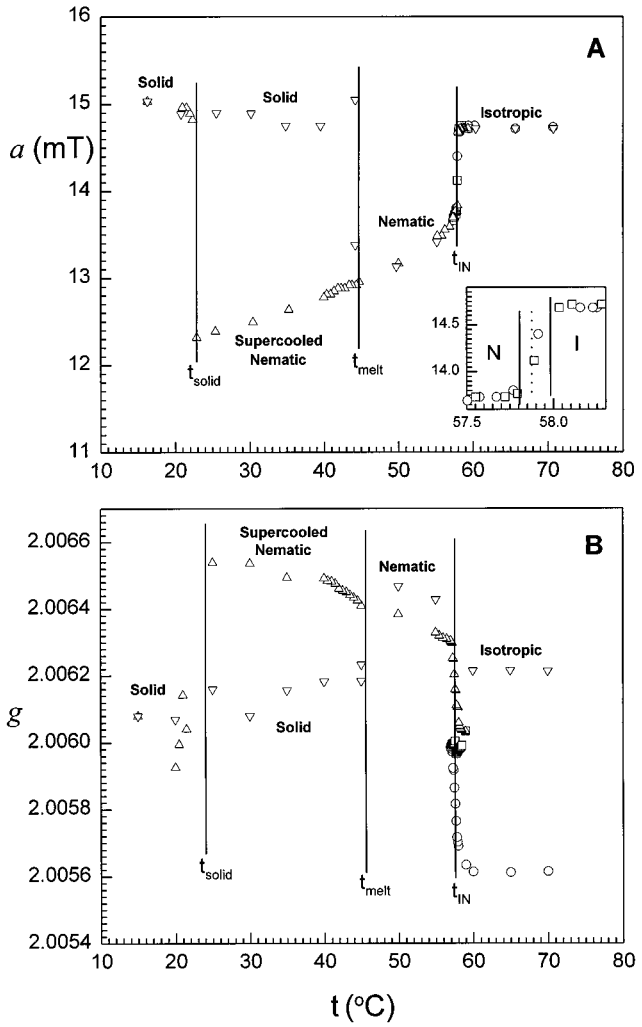

Figure 2. Hyperfine constant a (A) and the g-factor (B) versus temperature for PDT in 7CBz. The inset in (A) emphasizes the first cooling (○) and heating (□) cycles in the vicinity of the nematic-to-isotropic transition. The variation of a and the g-factor with temperature is given for the second cooling (△) and heating (▽) runs across the various phases.

crystal molecules; thus, the approach of their nitroxide groups to the polar ends of the liquid crystal molecules, i.e., the cyano groups, is closer on average than that encountered for PDT radical probes, giving rise to a higher hyperfine constant.

The results of this study, presented in Figures 1A, 2A, and 3A, show that the a_I value in the PDT/RCBz systems is identical to that for the PDT/RCB systems;[7] therefore, on average, the PDT radicals are similarly located relative to the solvent molecules in both systems. Clearly, the added central ester linkage in the RCBz molecules does not affect the proximity of the PDT probes to their tails. On the other hand, the results of this study (Figures 1B, 2B, and 3A′) show that the g-factor values of PDT in the isotropic phases of 6CBz (2.005 68) and 7CBz (2.005 62) are respectively lower than its reported[7,15] values in the isotropic phases of 6CB (2.006 66) and 7CB (2.006 33). This shift to lower g-factor values in the RCBz systems toward the g-factor value for the free electron spin (g_e = 2.002 32) reflects a greater π-delocalization in the RCBz solvent molecules resulting from the additional ester linkage to the benzene ring bearing the alkyl tail. The above interpretation of the a_I and g values for PDT in the RCB and RCBz solvents is in line with the theory proposed by Gendell et al.[16] that has been applied[7] to liquid crystal solvents.

The change in a ($\Delta a \equiv |a_I - a_N|$) at the isotropic-to-nematic transition temperature (t_{IN}) is the same in cooling and heating cycles for the PDT/6CBz (Figure 1A) and PDT/7CBz (Figure 2A) systems. However, the change in the g-factor ($\Delta g \equiv |g_I - g_N|$) at t_{IN} in the cooling cycle is different from its value for the heating cycle in both systems (Figures 1B and 2B). This is further clarified in Figure 3 for the 7CBz system. The following discussion on the 7CBz system using Figure 3 is also valid for the 6CBz system. The constancy of Δa and the identity of the a versus temperature plot over the different cooling and heating cycles (see Figure 3A−D) indicate that the part of the solvent molecule involved in the formation of the solvent−probe complex[7,16] has not been appreciably affected during the transition, where the value of Δa across the transition reflects only the change in order. On the other hand, Figure 3B′ clearly shows a general trend of increase in the g-factor with temperature interrupted by a small drop at t_{IN} of about 20% of the Δg observed in the first cooling cycle (Figure 3A′). The general rise in the g-factor and the persistence of Δg point to molecular and bulk changes, respectively. It is established that a decrease in order results in a decrease in the g-factor. Additionally an earlier study[7] on the RCB series indicates that the g-factor value is linked to the molecular structure of the probed solvent. Thus the unusual increase in the g-factor in the first heating cycle may be attributed to an ongoing conformational change triggered during the first cooling cycle to a conformer with lesser π-delocalization. Evidence of these competing effects on the g-factor is clear from the smallness of Δg in the first heating cycle relative to its value in the first cooling cycle. Evidence that the conformational change started during the first cooling cycle has not been reversed by the first heating cycle is afforded by the continued increase in the g-factor during the cooling of the isotropic phase and beyond t_{IN} in the second cooling cycle. Moreover, the g-factor values for the nematic phase in the second heating cycle fall in line with the g-factor values for the nematic phase in the second cooling cycle and, except for the small Δg in the first heating cycle, the Δg value across the nematic-to-isotropic transition is constant at about 0.000 22. The same Δg value has been obtained across the nematic-to-istropic transitions of the RCB liquid crystals. Thus a single liquid crystal conformer in a stable or metastable state would always give rise to a Δg close to 0.000 22 for a PDT probe and only during the conformational change will that Δg be masked by the above-mentioned competing molecular and bulk processes.

On cooling beyond t_{IN} (Figure 3C), the hyperfine constant a_N in the nematic and supercooled nematic phases decreases with temperature and is, as expected for the nitroxide radicals[17] and reported[7,8] for the PDT/RCB systems, smaller than a_I. However, at 23.1 °C, a temperature well below the melting point of 43.5 °C (Hoffmann-La Roche), the a value suddenly rises to a value comparable to a_I. The same behavior was observed in the PDT/6CB system (ref 7, Figures 2b), which had a narrower temperature range for the supercooled nematic region. The concomitance of this sudden increase in a by a sudden decrease in the g-factor value (Figure 3C,C′) indicates that an order−disorder transition has taken place. Such decrease in order suggests that the transition involves a conformational change in the liquid crystal molecule, which in turn disrupts the order of the supercooled nematic phase. On heating (Figure 3D,D′) the a and g-factor values return nearly to the same values obtained in the nematic region in the preceding cooling cycle (Figure 3C,C′) when a temperature close to the melting temperature reported by Hoffmann-La Roche is reached. This indicates that solidification must have taken place just after the

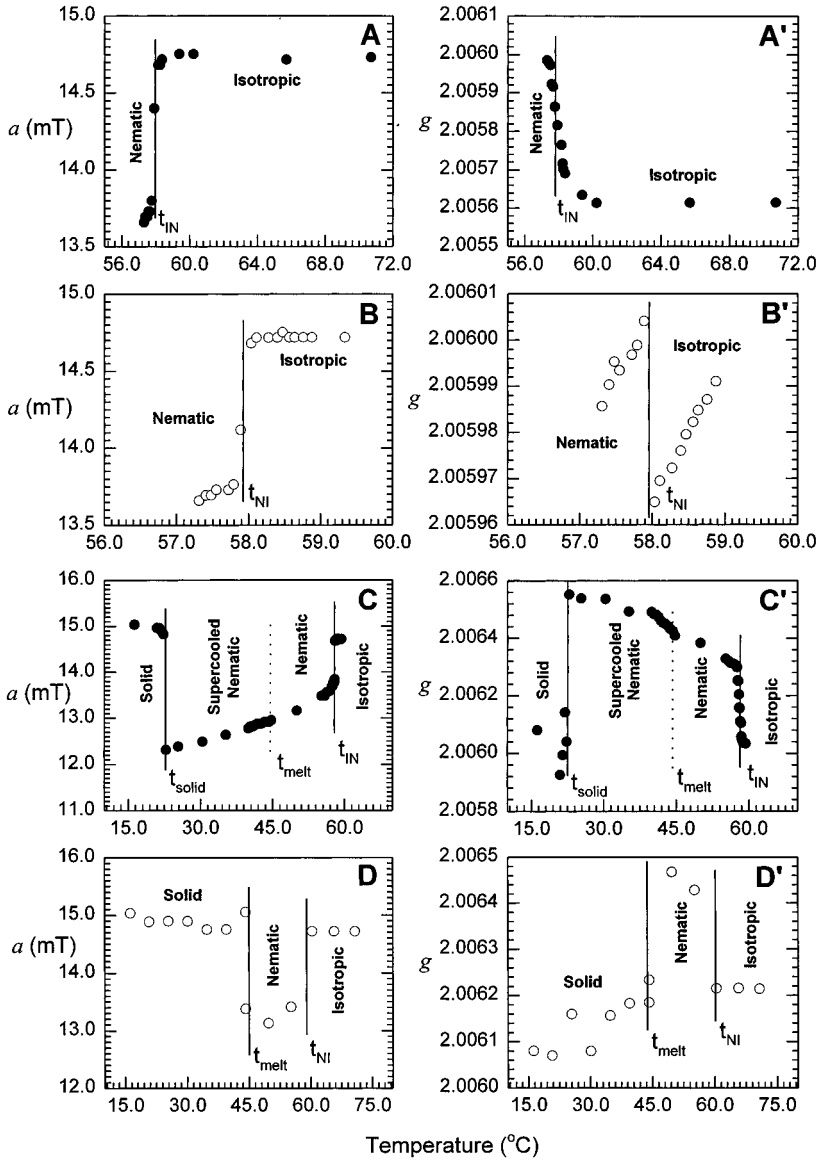

Figure 3. Hyperfine constant a (A−D) and the g-factor (A′−D′) versus temperature for PDT in the various phases of 7CBz. Cooling and heating runs are denoted by ■ and ○, respectively. The steps A−D (or A′−D′) reflect the order in which the experiment was done.

above-mentioned order−disorder transition. It is even likely that this conformational change is a prerequisite for solidification. It is hypothesized that at a low enough temperature the liquid crystal molecules revert to a conformation which, though individually stable at the molecular level, is disruptive to the bulk phase. It is likely that the necessary low temperature for such conformational change was not reached in systems where such order−disorder transition was not observed.[7] Further evidence for such conformational change preceding the solidification of the supercooled nematic phase has been sought in DSC experiments and molecular modeling using the ab initio Hartree−Fock method at the minimal STO-3G basis set.[12,13]

DSC Results. DSC cooling and heating thermograms at different rates for 6CB, 6CBz, and 7CBz are shown in Figure 4. For each of these liquid crystals the onset temperature of the nematic-to-isotropic transition on heating was equal to the onset temperature of the isotropic-to-nematic transition on cooling and independent of the heating or cooling rates. The peak for the nematic-to-isotropic transition of 6CBz was not observed at the heating rate of 10 °C/min owing to its proximity to the melting peak which is broad at that rate (Figure 4B′). These transition temperatures (Table 1) were more or less in agreement with the values quoted by the manufacturers (BDH for 6CB and Hoffmann-La Roche for 6CBz and 7CBz) and the transition temperatures obtained by EPR, which also were reproducible in heating and cooling cycles (insets in Figures 1A and 2A). The same constancy and independence of the rate has been observed for the temperature at the onset of melting for each of these liquid crystals (Figure 4A′−C′). On the other hand, each of these liquid crystals supercools and the onset temperature of its major solidification peak, which appears at a temperature much lower than its melting point, shifts to higher temperature as the cooling rate decreases (Figure 4A−C). This, the existence of several solidification peaks, which is clearly seen on expansion of the thermograms as illustrated for 7CBz in Figure 5, and, in the case of 6CBz and 7CBz, the appearance of a small endotherm on heating at about the same temperature at which the main solidification peak appears on cooling (Figures 4 and 5) indicate that a process of conformational change is going on during solidification. Clearly the solid associated with this peak is of a different structure from that which melts at the upper temperature.

Evidence for the existence of conformational change is provided by an endotherm preceding solidification on cooling,

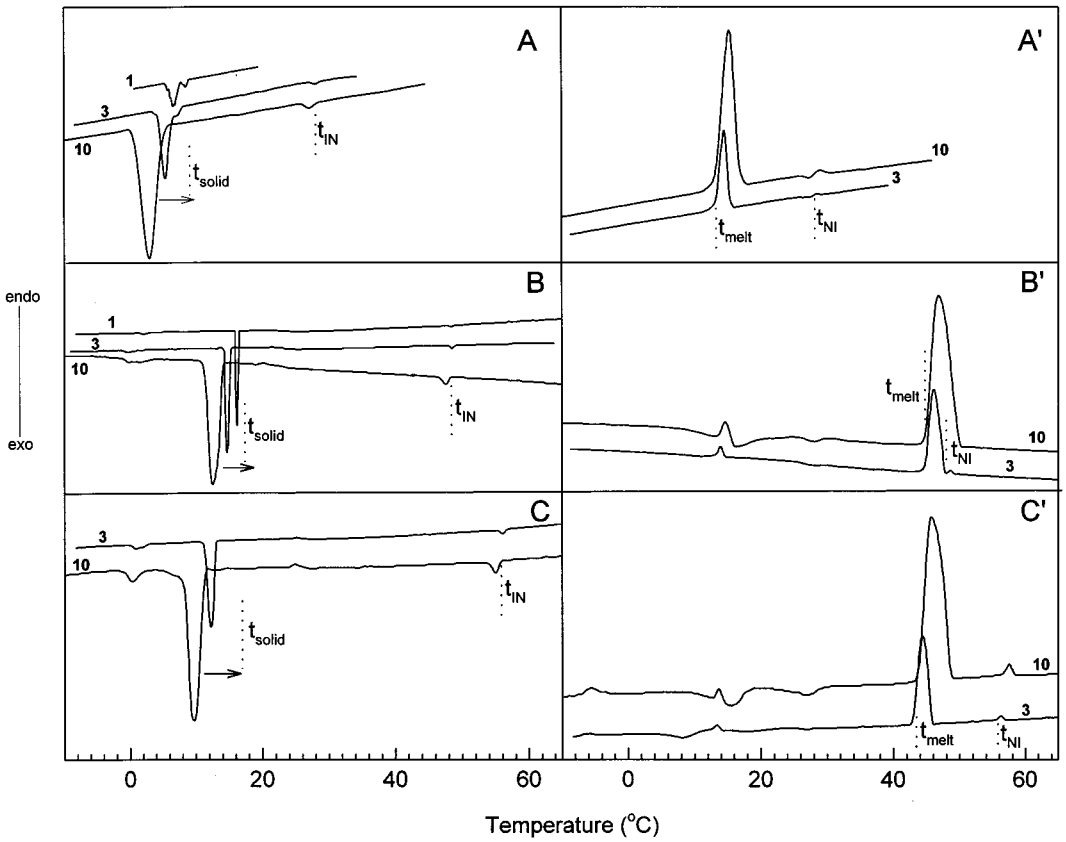

Figure 4. DSC cooling thermograms A, B, and C (and heating thermograms A′, B′, and C′) for 6CB, 6CBz, and 7CBz, respectively. The numbers on the thermograms are for heating or cooling rates in °C/min.

TABLE 1: Supercooled Nematic-to-Solid Transition Temperatures (t_{solid}), Solid-to-Nematic Transition Temperatures (t_{melt}), and Isotropic-to-Nematic Transition Temperatures (t_{IN}) for Liquid Crystals

liquid crystal	t_{solid} (°C)		t_{melt} (°C)			t_{IN} (°C)		
	DSC[b]	EPR	reported[c]	DSC	EPR	reported	DSC	EPR
6CB[a]	8.90	11.5	14.5	13.2	15.5	29	28.5	29.2
6CBz	16.45	17.3	44.5	44.8	45.5	48.0	48.6	48.8
7CBz	13.16	23.2	43.5	43.4	44.3	56.5	56.3	56.4

[a] EPR data for 6CB were taken from ref 7. [b] All the DSC data, except t_{solid} for 6CB and 6CBz, taken from thermograms at the cooling rate 1 °C/min, were collected from the thermograms at the rate 3 °C/min. [c] Reported transition temperatures quoted by the manufacturers (BDH for 6CB and Hoffmann-La Roche for 6CBz and 7CBz) and were measured using a polarizing microscope method.

at a temperature that is independent of the cooling rate, and which appears as a rate-independent exotherm at the same temperature and precedes melting on heating (Figures 4 and 5) for each of 6CBz and 7CBz. The order−disorder transition observed in the EPR experiment and described in the preceding section occurs on cooling at a temperature immediately succeeding this endotherm. The shift of the main solidification peak to higher temperatures to come closer to this endotherm as the cooling rate decreases (Figure 4A−C) and the manner in which the EPR spectra were taken (with a waiting time of at least 10 min. between runs, i.e., a cooling rate approaching zero) lead us to belief that an amorphous solid results from the order−disorder transition.

Evidence for transformations of different solid forms to the most stable solid form that melts at the temperature reported by the manufacturer is seen in Figure 5, which shows two heating rate-dependent exotherms in the vicinity of the above-

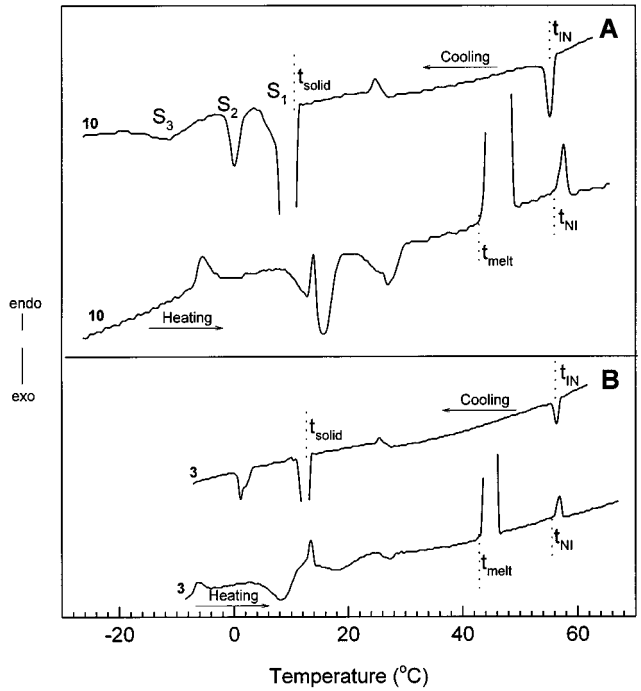

Figure 5. DSC cooling and heating thermograms for 7CBz at 10 and 3 °C/min expanded to show the solidification and melting of the different solid forms and endothermic and exothermic peaks in cooling and heating thermograms, respectively, at an onset temperature of about 26 °C.

mentioned temperature independent endotherm (at about 13 °C for 7CBz). As Figure 5 also shows there is another endotherm at about −6 °C for 7CBz. These endotherms and exotherms obtained while heating reflect a series of melting−solidification

TABLE 2: STO-3G Optimized Structural Parameters of 7CBz

bond lengths,[a] Å		bond angles,[a] deg		dihedral angles,[a] deg	
$r(C_2-C_1)$	1.395				
$r(C_3-C_1)$	1.383	$\angle(C_3-C_1-C_2)$	120.1		
$r(H_4-C_1)$	1.083	$\angle(H_4-C_1-C_2)$	119.8	$\tau(H_4-C_1-C_2-C_3)$	−179.9
$r(C_5-C_3)$	1.395	$\angle(C_5-C_3-C_1)$	120.1	$\tau(C_5-C_3-C_1-C_2)$	0.0
$r(C_6-C_2)$	1.396	$\angle(C_6-C_2-C_1)$	119.7	$\tau(C_6-C_2-C_1-C_3)$	−0.3
$r(C_7-C_2)$	1.461	$\angle(C_7-C_2-C_1)$	120.2	$\tau(C_7-C_2-C_1-C_6)$	−179.8
$r(H_9-C_3)$	1.082	$\angle(H_8-C_3-C_1)$	120.7	$\tau(H_8-C_3-C_1-C_5)$	179.8
$r(C_9-C_5)$	1.396	$\angle(C_9-C_5-C_3)$	120.0	$\tau(C_9-C_5-C_3-C_1)$	0.6
$r(O_{10}-C_5)$	1.406	$\angle(O_{10}-C_5-C_3)$	117.2	$\tau(O_{10}-C_5-C_3-C_9)$	175.2
$r(N_{11}-C_7)$	1.157	$\angle(N_{11}-C_7-C_2)$	179.9	$\tau(N_{11}-C_7-C_2-C_1)$	62.2
$r(H_{12}-C_6)$	1.083	$\angle(H_{12}-C_6-C_2)$	119.7	$\tau(C_{12}-C_6-C_2-C_1)$	−179.6
$r(C_{13}-O_{10})$	1.406	$\angle(C_{13}-O_{10}-C_5)$	115.4	**$\tau(C_{13}-O_{10}-C_5-C_3)$**	**129.5**
$r(H_{14}-C_9)$	1.082	$\angle(H_{14}-C_9-C_5)$	120.1	$\tau(H_{14}-C_9-C_5-C_3)$	179.4
$r(C_{15}-C_{13})$	1.515	$\angle(C_{15}-C_{13}-O_{10})$	111.4	$\tau(C_{15}-C_{13}-O_{10}-C_5)$	175.7
$r(O_{16}-C_{13})$	1.217	$\angle(O_{16}-C_{13}-O_{10})$	122.9	$\tau(O_{16}-C_{13}-O_{10}-C_{15})$	178.9
$r(C_{17}-C_{15})$	1.391	$\angle(C_{17}-C_{15}-C_{13})$	118.6	$\tau(C_{17}-C_{15}-C_{13}-O_{10})$	178.1
$r(C_{18}-C_{15})$	1.391	$\angle(C_{18}-C_{15}-C_{13})$	121.9	$\tau(C_{18}-C_{15}-C_{13}-C_{17})$	−180.0
$r(C_{19}-C_{17})$	1.383	$\angle(C_{19}-C_{17}-C_{15})$	120.2	$\tau(C_{19}-C_{17}-C_{15}-C_{13})$	−180.0
$r(C_{20}-C_{18})$	1.384	$\angle(C_{20}-C_{18}-C_{15})$	120.0	$\tau(C_{20}-C_{18}-C_{15}-C_{13})$	180.0
$r(H_{21}-C_{17})$	1.084	$\angle(H_{21}-C_{17}-C_{15})$	119.1	$\tau(H_{21}-C_{17}-C_{15}-C_{19})$	179.9
$r(H_{22}-C_{18})$	1.083	$\angle(H_{22}-C_{18}-C_{15})$	119.6	$\tau(H_{22}-C_{18}-C_{15}-C_{20})$	−179.9
$r(C_{23}-C_{19})$	1.393	$\angle(C_{23}-C_{19}-C_{17})$	120.7	$\tau(C_{23}-C_{19}-C_{17}-C_{15})$	0.07
$r(H_{24}-C_{19})$	1.082	$\angle(H_{24}-C_{19}-C_{17})$	119.7	$\tau(H_{24}-C_{19}-C_{17}-C_{23})$	179.8
$r(H_{25}-C_{20})$	1.082	$\angle(H_{25}-C_{20}-C_{18})$	119.6	$\tau(H_{25}-C_{20}-C_{18}-C_{15})$	−179.8
$r(C_{26}-C_{23})$	1.531	$\angle(C_{26}-C_{23}-C_{19})$	120.7	$\tau(C_{26}-C_{23}-C_{19}-C_{17})$	−178.8
$r(H_{27}-C_{26})$	1.088	$\angle(H_{27}-C_{26}-C_{23})$	109.4	$\tau(H_{27}-C_{26}-C_{23}-C_{19})$	−149.6
$r(H_{28}-C_{26})$	1.088	$\angle(H_{28}-C_{26}-C_{23})$	109.4	$\tau(H_{28}-C_{26}-C_{23}-H_{27})$	117.7
$r(C_{29}-C_{26})$	1.550	$\angle(C_{29}-C_{26}-C_{23})$	112.0	$\tau(C_{29}-C_{26}-C_{23}-H_{27})$	−121.2
$r(C_{30}-C_{29})$	1.545	$\angle(C_{30}-C_{29}-C_{26})$	112.1	$\tau(C_{30}-C_{29}-C_{26}-C_{23})$	−180.0
$r(H_{31}-C_{29})$	1.088	$\angle(H_{31}-C_{29}-C_{26})$	109.2	$\tau(H_{31}-C_{29}-C_{26}-C_{30})$	121.5
$r(H_{32}-C_{29})$	1.088	$\angle(H_{32}-C_{29}-C_{26})$	109.2	$\tau(H_{32}-C_{29}-C_{26}-C_{30})$	−121.5
$r(C_{33}-C_{30})$	1.544	$\angle(C_{33}-C_{30}-C_{29})$	112.3	$\tau(C_{33}-C_{30}-C_{29}-C_{26})$	−180.0
$r(H_{34}-C_{30})$	1.088	$\angle(H_{34}-C_{30}-C_{29})$	109.3	$\tau(H_{34}-C_{30}-C_{29}-C_{33})$	121.5
$r(H_{35}-C_{30})$	1.088	$\angle(H_{35}-C_{30}-C_{29})$	109.3	$\tau(H_{35}-C_{30}-C_{29}-C_{33})$	−121.5
$r(C_{36}-C_{33})$	1.545	$\angle(C_{36}-C_{33}-C_{30})$	112.4	$\tau(C_{36}-C_{33}-C_{30}-C_{29})$	−180.0
$r(H_{37}-C_{33})$	1.088	$\angle(H_{37}-C_{33}-C_{30})$	109.3	$\tau(H_{37}-C_{33}-C_{30}-C_{36})$	121.5
$r(H_{38}-C_{33})$	1.088	$\angle(H_{38}-C_{33}-C_{30})$	109.3	$\tau(H_{38}-C_{33}-C_{30}-C_{36})$	−121.5
$r(C_{39}-C_{36})$	1.545	$\angle(C_{39}-C_{36}-C_{33})$	112.4	$\tau(C_{39}-C_{36}-C_{33}-C_{30})$	180.0
$r(H_{40}-C_{36})$	1.088	$\angle(H_{40}-C_{36}-C_{33})$	109.3	$\tau(H_{40}-C_{36}-C_{33}-C_{39})$	121.5
$r(H_{41}-C_{36})$	1.088	$\angle(H_{41}-C_{36}-C_{33})$	109.3	$\tau(H_{41}-C_{36}-C_{33}-H_{39})$	−121.5
$r(C_{42}-C_{39})$	1.541	$\angle(C_{42}-C_{39}-C_{36})$	112.4	$\tau(C_{42}-C_{39}-C_{36}-C_{33})$	180.0
$r(H_{43}-C_{39})$	1.089	$\angle(H_{43}-C_{39}-C_{36})$	109.3	$\tau(H_{43}-C_{39}-C_{36}-C_{42})$	121.5
$r(H_{44}-C_{39})$	1.089	$\angle(H_{44}-C_{39}-C_{36})$	109.3	$\tau(H_{44}-C_{39}-C_{36}-C_{42})$	−121.5
$r(H_{45}-C_{42})$	1.086	$\angle(H_{45}-C_{42}-C_{39})$	110.6	$\tau(H_{45}-C_{42}-C_{39}-C_{36})$	180.0
$r(H_{46}-C_{42})$	1.086	$\angle(H_{46}-C_{42}-C_{39})$	110.7	$\tau(H_{46}-C_{42}-C_{39}-C_{45})$	120.0
$r(H_{47}-C_{42})$	1.086	$\angle(H_{47}-C_{42}-C_{39})$	110.7	$\tau(H_{47}-C_{42}-C_{39}-C_{45})$	−120.0

[a] Atom numbering as in Figure 5.

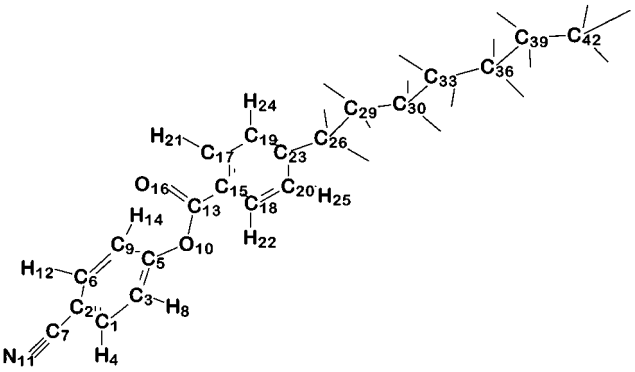

Figure 6. Fully optimized molecular structure for 7CBz from ab initio calculations using the STO-3G basis set.

steps in the direction of the most stable solid form. Such polymorphic transformations have been previously observed by Gray et al.[18] using a polarizing microscope with a heating stage and also confirmed by them using differential thermal analysis (DTA) in their studies of some polymorphic liquid crystals.

Ab Initio Calculation Results. The preceding experimental findings point to the existence of polymorphic solids, possibly arising from molecules of different conformations. Molecular modeling was performed to shed light on these conformers. Since the computational results for the 6CBz and 7CBz molecules were, except for very slight differences in the radii of the cavities occupied by the molecules and in the polarizabilities along the molecular axis, identical. The analysis of the ab initio calculations outlined below are for 7CBz.

The fully optimized structure for 7CBz (Figure 6 and Table 2) shows that in these molecules, the cyanophenyl portion and the alkylbenzoate portion are individually planar with a dihedral angle [$D = D_{13}(\tau(C_{13}-O_{10}-C_5-C_3)) - 180$] of −50.546° between them at their linkage point at the ester oxygen. This global-minimum molecular structure closely resembles the multiplanar molecular structure obtained from X-ray crystallography[19] where the planes of the phenyl rings are at a dihedral angle of 47.45°.

The search for other conformers due to the existence of the ester group involved the construction of a potential energy surface (PES)[14] by varying the dihedral angle D between the

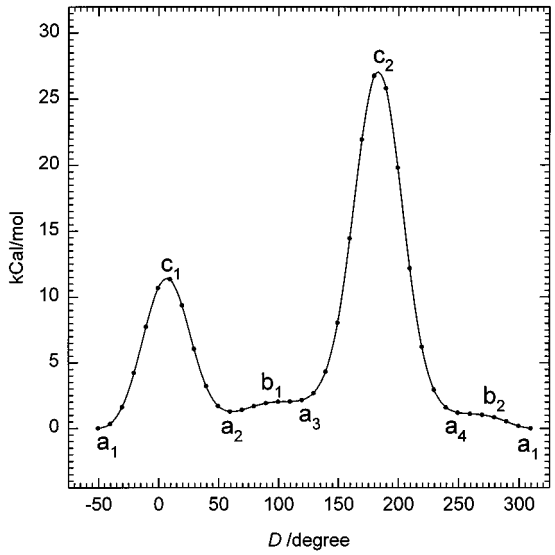

Figure 7. Potential energy surface diagram for 7CBz obtained from ab initio calculations using the STO-3G basis set.

planar portions of the global minimum structure in steps of 10° from −50.546 to +309.454° keeping all other molecular structure parameters constant. The PES[14] diagram resulting from this procedure is shown in Figure 7. The minima labeled a_2, a_3, and a_4 correspond, in the absence of the constraint mentioned below, to the optimized conformer that gives a minimum at a_1. Because of this same constraint each of the two maxima pairs labeled b_1 and b_2 and c_1 and c_2 corresponds to a conformer. The minor maxima at b_1 and b_2 correspond to a conformation where the planes of the cyanophenyl and alkylbenzoate portions are at 90° with respect to each other. The major maxima at c_1 and c_2 correspond to another conformation where the two portions of the molecule are in the same plane with respect to each other.

Having different minima or maxima values for a single conformer where only one should have been obtained results from the constraint applied in the calculation procedure. This constraint involved the fixing of atom positions relative to each other in each of the above-mentioned portions of the molecule during the scan to minimize the computational cost. This led to a distance of 1.653 Å between atoms H_{14} and O_{16} at the first planar position and a distance of 1.409 Å between atoms H_8 and O_{16} at the second planar position between the two portions. These different distances for what should have been identical arrangements within the molecule correspond, respectively, to the smaller and larger electronic repulsion giving rise to energies corresponding to c_1 and c_2 on the PES diagram in Figure 7. Thus, c_1 and c_2 correspond to the highly unstable conformer where the two portions of the molecule are in one plane, b_1 and b_2 correspond to a second slightly unstable conformer where the two portions are at a right angle with each other, and a_1-a_4 correspond to a third stable conformer where the planes of these portions are at about 50° with respect to each other. These conformers may account for the DSC results. It is also likely that the solidification peak obtained on cooling corresponds to trapping the least stable conformer in an amorphous solid form, which in turn reconforms on heating to the most stable conformer that melts at the upper melting temperature.

Conclusions

EPR studies using PDT as probe in the liquid crystals 6CBz and 7CBz show discontinuities in the *a* and *g*-factor values at their melting and nematic-to-isotropic transition temperatures and at the temperature of solidification of their supercooled nematic phases. These findings are in harmony with results previously obtained for the 6CB liquid crystal and suggest that the PDT probe is, on average, close to the alkyl tails of these liquid crystal solvent molecules.

The general increase in the *g*-factor during heating and cooling cycles in close succession in the vicinity of the isotropic-to-nematic (or nematic-to-isotropic) transition temperature that is superimposed on the Δg at the transition suggests a change in molecular structure alongside the change in the order of the bulk phase.

Evidence of conformational change upon solidification of the supercooled nematic phase is provided by the results of the DSC measurements. DSC thermograms on 6CBz and 7CBz reveal the existence of several solid forms and point to a conformational change in the molecules preceding or simultaneous with the solidification of their supercooled nematic phases. This conformational change gives rise to a disordered or "amorphous" solid. That this is the case is evident from the EPR experiment where the *a* values for PDT in this solid are comparable to the *a* values for PDT in the isotropic phase. Endothermic peaks and exothermic peaks obtained at the same temperature, in the region where a supercooled nematic exists, in cooling and heating runs, respectively, irrespective of the cooling or heating rates also suggest conformational changes.

Finally the ab initio calculations suggest three possible conformers for the RCBz liquid crystals. In the least stable conformer the cyanophenyl and the alkylbenzoate portions of the RCBz molecule are in one plane. The second conformer is slightly unstable with the above portions of the molecule at right angles to each other. For the most stable conformer the angle between the above portions is 50°. These molecular conformers may correlate with the polymorphic forms observed in the DSC experiment.

Acknowledgment. We thank King Fahd University of Petroleum and Minerals (KFUPM) for support of this work. We also express our thanks to Dr. H. Hamid, the manager of the Petroleum Refining and Petrochemicals Section at the KFUPM Research Institute (RI), for facilitating our use of the DSC-4 unit. We also thanks Mr. M. Saleem and Mr. I. A. Ismail for technical and experimental assistance.

References and Notes

(1) Collings, P. J. *Liquid Crystals: Nature's Delicate Phase of Matter*; Princeton University Press: Princeton, NJ, 1990.

(2) Williams, E. L. *Liquid Crystals for Electronic Devices*; John Wiley and Sons: New York, 1975.

(3) Chistyakov, I. G.; Usol'tseva, V. A. *Zhidkie kristally I ikh rol' v meditsine I biologii (Liquid Crystals and their Role in Medicine and Biology)*; Ivanovo: 1962.

(4) Mishra, R. K. *Mol. Cryst. Liq. Cryst.* **1975**, *29*, 201.

(5) Tsykalo, A. L. *Thermophysical Properties of Liquid Crystals*; Gorden and Breach Science Publishers: Amsterdam, 1991.

(6) Blinov, L. M. *Usp. Fiz. Nauk* **1974**, *114*, 67 [*Sov. Phys. Usp.* **1975**, *17*, 658].

(7) Morsy, M. A.; Oweimreen, G. A.; Hwang, J. S. *J. Phys. Chem.* **1996**, *100*, 8533 and references therein.

(8) Hwang, J. S.; Morsy, M. A.; Oweimreen, G. A. *J. Phys. Chem.* **1994**, *98*, 9056.

(9) HyperChem, Ver. 4 Runs under Microsoft Windows, Hypercube, Waterloo, Ontario, Canada, 1994.

(10) Alliger, N. L. *J. Am. Chem. Soc.* **1977**, *99*, 8127.

(11) Stewart, J. J. *P. MOPAC: J. Comput.-Aided Mol. Des.* **1990**, *4*, 1−105.

(12) Frisch, M. J.; Trucks, G. W.; Schlegel, H. B.; Gill, P. M. W.; Johnson, B. G.; Robb, M. A.; Cheeseman, J. R.; Keith, T.; Petersson, G. A.; Montgomery, J. A.; Raghavachari, K.; Al-Laham, M. A.; Zakrzewski,

V. G.; Ortiz, J. V.; Foresman, J. B.; Peng, C. Y.; Ayala, P. Y.; Chen, W.; Wong, M. W.; Andres, J. L.; Replogle, E. S.; Gomperts, R.; Martin, R. L.; Fox, D. J.; Binkley, J. S.; Defrees, D. J.; Baker, J.; Stewart, J. P.; Head-Gordon, M.; Gonzalez, C.; Pople, J. A. *Gaussian 94*, Revision B.2; Gaussian, Inc.: Pittsburgh, PA, 1995.

(13) (a) Hehre, W. J.; Stewart, R. F.; Pople, J. A. *J. Chem. Phys.* **1969**, 51, 2657. (b) Collins, J. B.; Schleyer, V. R.; Binkley, J. S.; Pople, J. A. *J. Chem. Phys.* **1976**, *64*, 5142.

(14) We retained the term potential energy surface (PES) used in Foresman and Frisch. Foresman, J. B.; Frisch, A. (*Exploring Chemistry with Electronic Structure Methods: A Guide to Using Gaussian*) 2nd ed.; Gaussian Inc.: Pittsburgh, PA, 1996). In actual fact what is referred to here is a potential energy curve, i.e., a slice off a potential energy surface.

(15) Morsy, M. A.; Hwang, J. S.; Oweimreen, G. A. *J. Phys. Chem. B* **1997**, *101*, 2120.

(16) Gendell, J.; Freed, J. H.; Fraenkel, G. K. *J. Chem. Phys.* **1962**, *37*, 2832.

(17) Rao, K. V.; Hwang, J. S.; Freed, J. H. *Phys. Rev. Lett.* **1979**, *37*, 515.

(18) Gray, G. W.; Harrison, K. J.; Nash, J. A.; Constant, J.; Hulme, D. S.; Kirton, J.; Raynee, E. P. In *Proceedings of the Symposium on Ordered Fluids and Liquid Crystals*; Porter, R. S., Johnson, J. F., Eds.; 1974; p 617.

(19) Mandal, P.; Paul, S.; Schenk, H.; Goubitz, K. *Mol. Cryst. Liq. Cryst.* **1986**, *135*, 35.